Journal of Thermal Analysis and Calorimetry, Vol. 83 (2006) 2, 313–319

ISOTHERMAL CRYSTALLISATION KINETICS OF POLY(3-HYDROXYBUTYRATE) USING STEP-SCAN DSC

*L. M. W. K. Gunaratne and R. A. Shanks**

School of Applied Science, RMIT University, GPO Box 2476V, Melbourne, VIC 3001, Australia

The crystallisation kinetics, melting behaviour and morphology, of bacterial poly(3-hydoxybutyrate) (PHB) have been investigated by using differential scanning calorimetry (DSC), step-scan DSC (SDSC), wide angle X-ray diffraction (WAXRD) and hot stage polarised optical microscopy (HSPOM). DSC imparted isothermal crystallisation thermal history. The subsequent melting behaviour revealed that all PHB materials experienced secondary crystallisation during heating and the extent of secondary crystallisation varied depending on the crystallisation temperature. PHB samples were found to exhibit double melting behaviour due to melting of SDSC scan-induced secondary crystals, while considerable secondary crystallisation or annealing took place under the modulated heating conditions. The overall melting behaviour was rationalised in terms of recrystallisation and/or annealing of crystals. Interestingly, the PHB materials analysed by SDSC showed a broad exotherm before the melting peak in the non-reversing curve and a multiple melting peak reversing curve, verifying that the melting-recrystallisation and remelting process was operative. HSOM studies supported the conclusions from DSC that the radial growth rate of the PHB spherulites was significantly varied upon the crystallisation conditions. One form of crystals was shown by WAXRD from isothermally crystallised PHB.

Keywords: *isothermal crystallisation, morphology, poly(3-hydroxybutyrate), step-scan DSC, wide angle X-ray diffraction*

Introduction

Poly(3-hydroxybutyrate) (PHB) is a naturally occurring biopolyester having the chemical structure $[–OCH(CH_3)CH_2(C=O)–]_n$. PHB was first discovered in 1925 by Lemoigne [1]. PHB is usually produced by bacterial fermentation, and its biological function is similar to that of glycogen in mammalian systems and starch in plants [2]. PHB was introduced as a commercial product by ICI Pty Ltd for biotechnology biodegradable plastic moulded products [3]. PHB has attracted enormous attention in agriculture, pharmaceutical and medical industries due to its biocompatibility and biodegradability. Since PHB degrades in all environments, it has been proposed for the packaging industry as a biodegradable polymer to minimise environmental pollution. PHB is a controversial polymer with many interesting characteristics. Its continuing interest as a commercial biopolymer and its various thermal and mechanical properties have been made the subject of many studies [4–7]. PHB is a crystalline thermoplastic polymer with a relatively high melting temperature, T_m=170–180°C, and a glass transition temperature in the range of 0–5°C. PHB undergoes thermal degradation at temperatures near the melting temperature [4, 8]. PHB of natural origin has perfect stereoregularity, high purity and a high degree of crystallinity so that it has been considered for study of isothermal crystallisation kinetics and morphology [9]. PHB has low nucleation density and crystallises slowly to form large spherulites [10].

Differential scanning calorimetry (DSC) is an important technique that is used to study melting and crystallisation behaviour and the morphology of polymers. However, the interpretation of a DSC scan is often ambiguous due to many effects (recrystallisation, reorganisation and annealing) simultaneously occurring during heating. Temperature modulated differential scanning calorimetry (TMDSC) techniques, such as modulated differential scanning calorimetry (MDSC) and step-scan differential scanning calorimetry (SDSC) have been recently established as alternative techniques to produce new and different information on thermal transition of polymers relative to conventional DSC [11–15]. TMDSC has been extensively described elsewhere [12–19]. TMDSC uses a periodic temperature modulation over a traditional linear heating or cooling ramp and is capable of giving accurate heat capacity measurements and separating underlying kinetic and thermodynamic phenomena with better resolution and sensitivity.

In these experiments, there are two main approaches to analyse the resulting modulated heat flow: The reversing/non-reversing (NR) total heat flow or heat capacity approach as described by Reading *et al*. [12] and the complex heat capacity approach by Schawe [13]. Despite the methods used, three types

* Author for correspondence: robert.shanks@rmit.edu.au

1388–6150/$20.00

Akadémiai Kiadó, Budapest, Hungary
Springer, Dordrecht, The Netherlands

of curves can normally be derived from the modulated DSC experiments: total heat flow or heat capacity curve (total C_p, same as conventional DSC curve), in-phase curve (reversing or storage) and out-of-phase curve (kinetic or loss) [20, 21]. In addition, the non-reversing heat capacity curve (NRC_p) can be obtained by the difference between the total C_p and reversing heat capacity (C'_p). This curve is particularly useful for determining irreversible processes such as enthalpy relaxation, evaporation, cold crystallisation, chemical reactions, curing, decomposition and recrystallisation. The reversing curve represents the effects that are thermodynamically reversible at the time and temperature at which they are detected, whereas the out-of-phase curve is expected to show irreversible phenomena within the modulation conditions.

SDSC technique has recently become available and developed as a simplified version of TMDSC [11, 22, 23]. It utilises a heat–isothermal (or cooling–isothermal) program, where the isothermal segment continues until the heat flow is decreased to within a predetermined set-value (criteria). The apparent thermodynamic response only occurs during the heating (or cooling) segment and reflects the reversing changes of the polymer. The kinetic response yields the kinetic processes that are extracted from the isothermal segment. The equation that describes the heat flow response is given by

$$dQ/dt = C_p(dT/dt) + f(t,T) \quad (1)$$

where, dQ/dt is the heat flow, C_p is the heat capacity, dT/dt is the heating rate and $f(t,T)$ is the kinetic response. The interpretation of results is similar to MDSC, and the reversing (so-called thermodynamic C_p signal, reversible under the experimental conditions) and non-reversing (Isok baseline, kinetic response) contributions can be directly extracted from data.

Since PHB is slow to reach crystallisation equilibrium, its thermal history can be readily controlled by the crystallisation conditions. PHB is brittle in nature. De Koning *et al*. have shown that PHB can undergo physical ageing during the storage at room temperature increasing its brittleness [24]. The phenomenon of secondary crystallisation of initially formed crystals has been suggested, and researchers have also shown that PHB can be toughened by annealing [24, 25] and crack-free spherulites can be grown from the melt by controlling the crystallisation conditions [26]. In this paper, the influence of thermal history is explored using isothermal crystallisation conditions. The melting of PHB is studied using step-scan DSC conditions. A morphological study of PHB is carried out using wide angle X-ray diffraction (WAXRD) and hot stage polarised optical microscopy (HSPOM) with isothermal crystallisation condition analogous to the DSC crystallisation treatments.

Experimental

Sample preparation

Bacterial PHB was obtained from Sigma Aldrich Chemicals, Australia as a white powder (M_w=2.3·10^5 g mol^{-1} and M_n=8.7·10^4 g mol^{-1} [27]). PHB (1 g) was dissolved in 100 mL of chloroform and filtered by vacuum filtration to remove any insoluble fraction or impurities. Semi-crystalline films were obtained by solvent casting at room temperature. The resulting films (~60 μm thick) were further dried in vacuum at 50°C for 3 h to remove residual solvent and moisture. Films were stored in a desiccator under nitrogen atmosphere prior to use.

Differential scanning calorimetry and step-scan DSC

Thermal treatments and measurements were performed using a Perkin-Elmer Pyris 1 DSC (Pyris software 3.81) operated at subambient temperature mode with an Intracooler 2P. With the Pyris 1 DSC, isoscan, heat-cool and step-scan modes are available. About 2–3 mg of PHB film was sealed in a 10 μL aluminium pan, and all scans were carried out under nitrogen (20 mL min^{-1}). High purity indium and octadecane were used for temperature calibration and indium was used for calibration of heat flow. Furnace and specific heat calibration was performed according to the manufacturer instructions.

PHB was melted at 190°C for 5 min to destroy any previous thermal history, then in order to avoid crystallisation or under cooling, the samples were cooled to 5°C above each isothermal crystallisation temperature from 190°C at a nominal rate of 200°C min^{-1} and then cooled to selected temperatures at 20°C min^{-1}. PHB was treated isothermal crystallisation condition at selected temperatures (105, 110, 115 and 120°C) for 60 min. The SDSC heating scans of the treated samples were then obtained from the crystallisation temperature to 190°C at an average rate of 2°C min^{-1} with a period of 60 s (temperature increment of 2°C with each 30 s isothermal and scanning segments). From the SDSC melting scans, melting temperature (T_m) and enthalpy of fusion (ΔH_m) were determined. The data for isothermal segments were collected within the 0.005 mW s^{-1} criteria. Specific heat calculation for heat flow response was carried out using the area under each segment of the curve. For each scan, a baseline was recorded with matched empty aluminium pans using the same method. All SDSC curves were corrected using the appropriate baselines recorded under identical conditions and converted to specific heat capacity curves. The crystallinity was calculated using the equation,

$$X_{cPHB} = \Delta H_{PHB}/\Delta H^0_{PHB} \quad (2)$$

where ΔH^0_{PHB} is the enthalpy of melting of pure crystals 146 J g^{-1} [28] and ΔH_{PHB} the measured enthalpy of melting for PHB.

Wide angle X-ray diffraction

Wide-angle X-ray diffraction measurements were carried out on a Bruker AXS X-ray generator (D8 Advance model) using CuK_α radiation (wavelength 0.1542 nm) operated at 20 kV and 5 mA. The scattering angle (2θ) covered the range from 10 to 38° (θ is Bragg angle) at a step of 0.02° and sampling interval of 10 s. Films of PHB were isothermally crystallised for 60 min at similar temperatures (105, 110, 115 and 120°C) as used for DSC treatments on the X-ray instrument hot stage platform. These samples were melted at 190°C for 5 min after heating from room temperature at 40°C min^{-1} and then cool to selected temperature at 200°C min^{-1}.

Optical microscopy

The crystal morphologies of PHB were observed using a Nikon Labophot 2 polarising optical microscope with a Mettler FP90 hot stage and images were captured using Nikon digital camera. Each PHB film was mounted on a glass slide under a cover slip. The specimens were first heated on a hot-stage from room temperature to 190°C at a rate of 20°C min^{-1} and maintained at this temperature for 3 min before cooling. The morphological studies of polymers were carried out using isothermal crystallisation at selected temperature for 60 min after cooling at 20°C min^{-1} rate from 190°C under nitrogen atmosphere. PHB was isothermally crystallised at 105, 110, 115 and 120°C to observe morphological behaviour of PHB comparable to DSC crystallisation.

Results and discussion

Isothermal crystallisation kinetics from DSC analysis

Figure 1 shows the isothermal crystallisation exotherms of PHB at different crystallisation temperatures. The crystallisation process was completed in less than 30 min. As crystallisation temperature was increased the crystallisation peak of the exotherm moved to longer times and became broader. The relative crystallinity, X_t, after time t, was calculated from the equation,

$$X_t = \int_0^t (dH/dt)dt \Big/ \int_0^\infty (dH/dt)dt \qquad (3)$$

where the first integral is the heat generated after time t and the second integral is the total heat of crystallisation for $t = \infty$. Figure 2a shows X_t *vs*. time for PHB at each

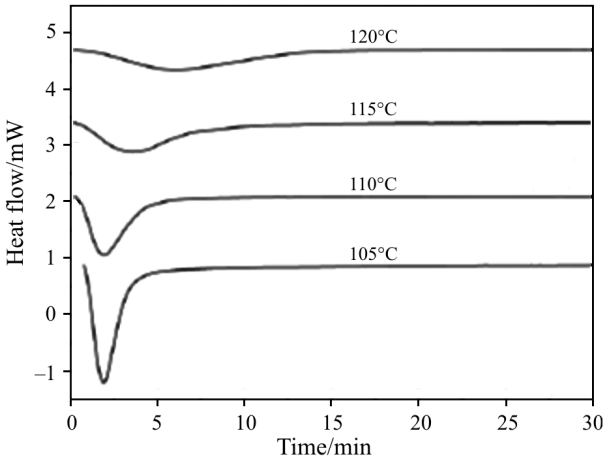

Fig. 1 Heat flow *vs*. time during isothermal crystallisation of PHB at various crystallisation temperatures

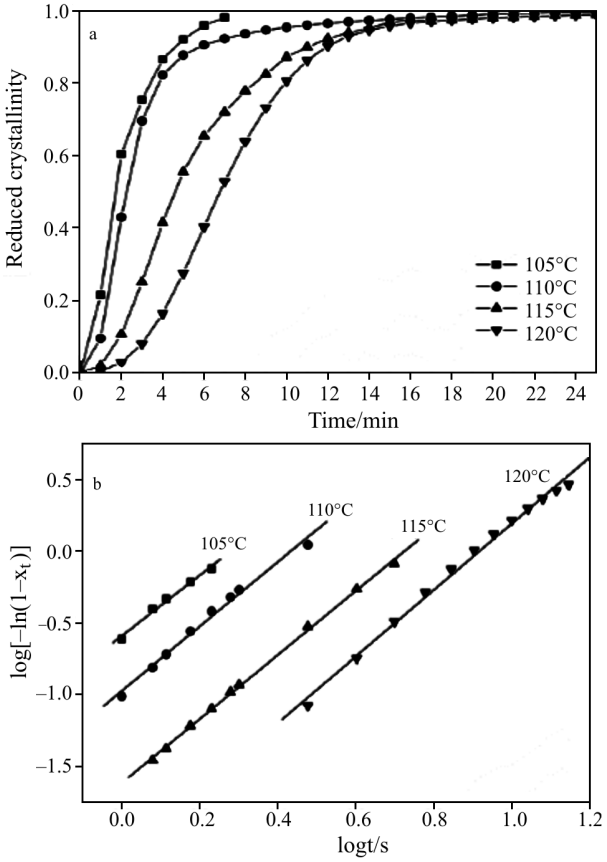

Fig. 2 a – Reduced crystallinity (X_t) *vs*. time of PHB at different crystallisation temperatures; b – plot of log[–ln(1–X_t)] *vs*. log*t* for isothermal crystallisation at the indicated temperatures

isothermal temperature. The rate of crystallisation was obtained from the slope of each curve [29]. The linear region was between 20 to 60% relative crystallinity, proved that the rate of crystallisation was constant. The rate of crystallisation (V_c) was calculated from linear re-

gion of the curve [30]. The activation energy of the overall process can be calculated from the V_c using the equation,

$$V_c = A\exp(-E/RT) \quad (4)$$

where A, E, R and T are the pre-exponential factor, activation energy (J mol^{-1}), universal gas constant (8.314 J mol^{-1} K^{-1}) and crystallisation temperature (K), respectively. E was calculated from the slope of $\ln V_c$ *vs*. $1/T$ curve and the values are listed in Table 1. The value of 87 kJ mol^{-1} is closer to that of PHB isothermally crystallised at lower temperature [31].

The crystallisation half time ($t_{1/2}$ – time required to reach X_t=0.5) of PHB calculated from crystallisation exotherms, are listed in Table 1. As shown in Fig. 1 the $t_{1/2}$ values increased with increasing crystallisation temperature.

Table 1 The crystallisation rate (V_c) and activation energy (E) values of the overall process of crystallisation of PHB

Polymer	T_c/K	V_c/min^{-1}	$t_{1/2}$/min	E/kJ mol^{-1}
PHB	378	0.33	1.65	
	383	0.30	2.31	
	388	0.15	4.55	
	293	0.12	6.78	87.3

The isothermal crystallisation kinetics of PHB was analysed using the Avrami equation [32, 33].

$$1-X_t = \exp(-kt^n) \quad (5)$$

Equation (5) can be written as,

$$\log[-\ln(1-X_t)] = \log k + n\log t \quad (6)$$

where X_t, k, n and t are mass fraction crystallinity, rate constant, Avrami exponent and time of crystallisation, respectively. Both k and n depend on the mechanism of the nucleation as well as the growth geometry. Avrami plots of PHB at different crystallisation temperatures are shown in Fig. 2b. Experimental data fit well with the Avrami equation at different T_c. Avrami exponent (n) and overall crystallisation rate constant (k) were calculated from Avrami curves and listed in Table 2. Furthermore the crystallisation half time ($t_{1/2}$) was obtained from following equation and data included in Table 2.

Table 2 The values of n, k, $t_{1/2}$ and g of PHB

T_c/°C	n	k	$t_{1/2}$/min	g/min^{-1}
105	2.12	0.2376	1.657	0.6035
110	2.25	0.1060	2.304	0.4340
115	2.23	0.0236	4.552	0.2197
120	2.32	0.0082	6.775	0.1476

$$t_{1/2} = (\ln 2/k)^{1/n} \quad (7)$$

In addition, the calculated values of the half-time ($t_{1/2}$) (Table 2) are in agreement with values obtained directly from heat flow curves (Table 1). The rate of crystallisation (g) calculated from the reciprocal of crystallisation half time, listed in Table 2, was decreased with increasing temperature. The rate of crystallisation g increased with supercooling, if the phase transition in crystallisation is nucleation controlled [34]. This was observed and agreed well with this argument.

$$g = (t_{1/2})^{-1} \quad (8)$$

The rate constant k, which is dependent on both the nucleation mechanism and the growth rate, decreased with increasing T_c. The n is about 2 for all selected temperatures and both nucleation behaviour and geometry of crystal growth of PHB are not affected by T_c. According to our results the Avrami exponent, n=2 for pure PHB within this temperature interval, corresponds to two-dimensional (2D) spherulite growth and heterogeneous nucleation. The nucleation growth of PHB and effect of nucleation agent had been studied by Barham [35].

Melting behaviour using step-scan DSC

Figure 3 shows apparent thermodynamic heat capacity ($C_{p,ATD}$) and isoK baseline heat capacity ($C_{p,IsoK}$) specific heat capacity curves derived from SDSC iso-scan heating curves of PHB, with 2°C min^{-1} average heating rate after isothermal crystallisation at 105, 110, 115 and 120°C (PHB-105, PHB-110, PHB-115 and PHB-120, respectively) for 60 min. The corresponding thermal data: melting temperatures, enthalpies and crystallinity are listed in Table 3. The irreversible event of recrystallisation exothermic peaks are present in the $C_{p,IsoK}$ curves. Multiple melting peaks were obtained in all $C_{p,ATD}$ curves except PHB-105. PHB showed a melting peak at 171.8°C, while the $C_{p,IsoK}$ shows a broad exothermic peak before melting (at about 167°C, indicated by an arrow) and unresolved double melting endothermic peaks at 173.3 and 177.7°C. The $C_{p,ATD}$ curves of PHB-110, PHB-115 and PHB-120 showed one melting peak with a shoulder on the upper temperature side of the peak, where as $C_{p,IsoK}$ showed an exothermic peak before melting, followed by melting peak, except PHB-110. As the crystallisation temperature increased, the lower melting peak of $C_{p,IsoK}$ shifted to higher temperatures. In particular, the height of the higher melting peak decreased with increasing crystallisation temperature and disappeared above 115°C. Above 115°C, all of the melting peaks of $C_{p,IsoK}$ curves merged into a single peak and shifted to higher temperature. Similar behaviour was reported for poly(ethylene 2,6-naphthalate) [36] and poly(ethylene 2,6-naphthalenedicarboxylate)

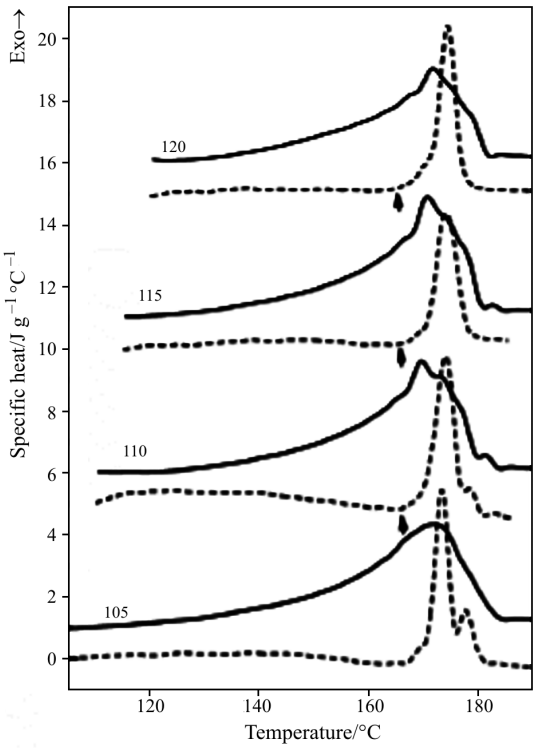

Fig. 3 SDSC melting curves of PHB after isothermal crystallisation at various temperatures (an adapted scale is drawn by adding 5 units to each curve)

[37] using conventional DSC. The large and low melting peak of $C_{p,IsoK}$ corresponded to the melting of initial crystals formed during isothermal crystallisation and the higher endotherm attributed to the melting of crystals generated by melt recrystallisation during SDSC melting scan.

The exothermic peak of the $C_{p,IsoK}$ curve in Fig. 3 suggested that PHB provided significant recrystallisation and/or annealing throughout the SDSC heating period. Due to the overlap of the recrystallisation exotherm and the melting endotherm, the recrystallisation exotherm is not observed in a conventional DSC scans after isothermal crystallisation of poly(ethylene 2,6-naphthalate) [36]. The reversing contribution was considerably decreased with increasing crystallisation temperature due to slow growth rate of crystals at higher temperatures.

$C_{p,ATD}$ curves showed unresolved melting peaks, whereas $C_{p,IsoK}$ signals provided exothermic peaks in the melting region suggesting the presence of a melting-recrystallisation-remelting (mrr) process. An endothermic peak was also observed in the $C_{p,IsoK}$ curves. As the crystallisation temperature increased, T_m was shifted towards higher temperatures (Table 3) suggesting that crystals grown slowly provide crystals with increased thermal stability compared with the crystals formed faster at lower temperatures. The recrystallisation process of PHB–PVAc, PET and PEEK were reported during conventional DSC heating after isothermal crystallisation [31, 38, 39].

Double or multiple behaviours are common for PHB and its copolymers depending on the crystallisation conditions [40]. Multiple melting behaviour of a polymer is generally proposed to link either to the process of mrr or to melting of crystals with different lamellar thickness and/or different crystal morphology [41]. It has been observed that the mrr behaviour operated for melt isothermally crystallised PHB. The results suggested that the amount of recrystallisation during heating was less for slowly formed crystals at higher crystallisation temperatures. Isothermally crystallised PHB at higher temperature are shown by relatively well-organised lamellae, which undergo less rearrangement.

Wide angle X-ray diffraction

Figure 4 shows WAXRD curves of the PHB after isothermally crystallised at 105, 110, 115 and 120°C for 60 min. The spherulites crystallised at 105°C show crystalline reflections of the (020), (100), (110) and (002) planes (2θ is 13, 16, 17 and 30°, respectively), which are major reflections of the β-form crystal. Considering WAXRD results and HSPOM results, it is supported that PHB crystallised at all temperatures have β-form crystals. 2θ=17° corresponding to the (110) diffraction of PHB type lattice [42]. WAXRD curves provided similar peaks but with dif-

Table 3 Thermal data for isothermally crystallised PHB after SDCS melting

Polymer	T_m ($C_{p,ATD}$)/°C	ΔH_m ($C_{p,ATD}$)/J g^{-1}	T_m ($C_{p,IsoK}$)/°C	ΔH_m ($C_{p,IsoK}$)/J g^{-1}	X_c*
PHB-105	171.8	71.7	173.3 177.7	21.7	0.49
PHB-110	169.6 173.2	67.9	174.1 178.4	19.9	0.47
PHB-115	170.7 174.2	66.9	174.1	19.6	0.46
PHB-120	171.7 175.0	52.3	174.4	20.8	0.36

*X_c was calculated from ΔH_m ($C_{p,ATD}$)

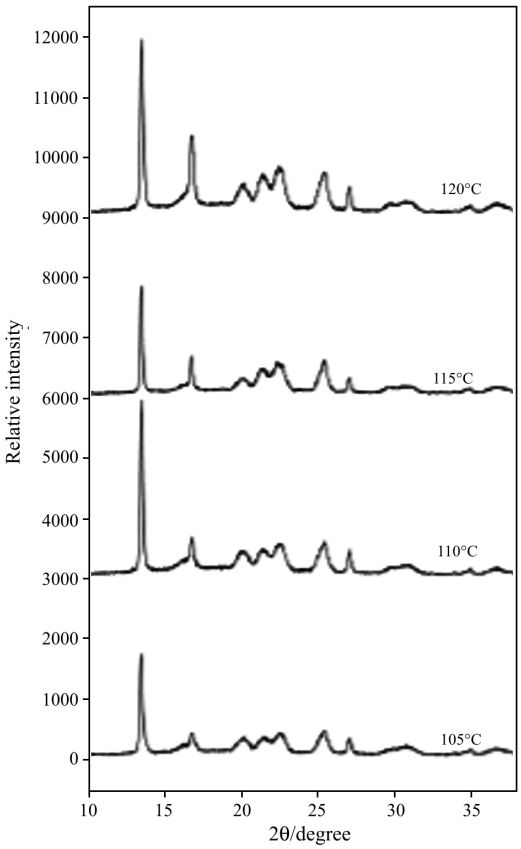

Fig. 4 Wide angle X-ray diffraction of PHB after isothermal crystallisation at various temperatures (an adapted scale is drawn by adding 3000 units to each curve)

ferent intensities and peak widths confirm that the influence of crystal growth rate and size of the crystals with selected crystallisation temperatures.

Morphological studies

The crystal morphology of PHB was observed by polarised optical microscopy after isothermal crystallisation at 105, 110, 115 and 120°C for 60 min. As illustrated in Fig. 5, crystal morphologies were obtained under similar crystallisation condition. All images showed the characteristic larger spherulites that contain a Maltese cross-birefringent pattern and concentric extinction bands [43]. A sharp fibril structure growing radially with a large radius was seen for isothermally crystallised PHB at 105°C (Fig. 5a). Figures 5b, c and d show the polarised optical microscopy images of PHB isothermally formed at 110, 115 and 120°C after 20°C min^{-1} cooling from the melt. These treatments were performed analogous to the DSC and WAXRD crystallisation treatments of this polymer (curves 105 to 120°C of Fig. 1 and curves 105 to 120°C of Fig. 4, respectively). Slow crystallisation at a higher temperature with low nucleation density permitted large crystals to grow, whereas faster crystallisation resulted in

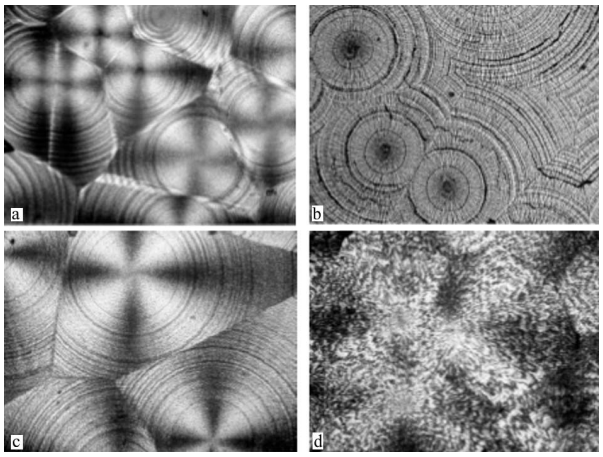

Fig. 5 Polarised optical micrographs of PHB after isothermal crystallisation at a – 105, b – 110, c – 115 and d – 120°C (×100)

smaller crystal size induced by increased nucleation density within selected temperatures. Thus, the PHB crystallised at higher temperatures have larger spherulites than at lower temperatures. These findings are consistent with the large individual spherulites of PHB previously observed [4, 43]. Separation and regularity of bands varied with crystallisation methods and conditions [44]. Isothermal and slow-cooled samples provided a large average spherulite radius indicating a low nucleation density [45]. It is these large spherulites that are responsible for the brittleness of PHB [46]. These results provided clear evidence of crystal growth dependence of PHB on isothermal crystallisation at selected temperatures.

Conclusions

The overall isothermal crystallisation kinetics and melting behaviour of PHB, were studied by SDSC. The Avrami analysis indicates that the increases of crystallisation temperature of PHB decrease the crystallisation rate of the PHB phase, but does not affect PHB nucleation mechanism and geometry of crystal growth. Multiple melting endotherms were obtained in both $C_{p,ATD}$ and $C_{p,IsoK}$ and exotherms were observed in $C_{p,IsoK}$ caused by recrystallisation during the SDSC heating. The lower melting peak was due to melting of primary crystals formed during the isothermal crystallisation process and the second melting peak was attributed to recrystallisation during SDCS heating. The SDSC method separated thermodynamic and kinetic contributions without Fourier transformation, by step-wise measurement of specific heat. Different morphologies obtained by HSPOM confirmed the effect of crystallisation rate and nucleation density of the PHB crystallised at selected temperatures by isothermal crystallisation condition.

References

1 A. EI-Hadi, R. Schanabel, E. Straube, G. Muller and S. Henning, Polymer Testing, 21 (2002) 665.
2 S. Bloembergen and D. A. Holden, Macromolecules, 19 (1986) 2865.
3 P. A. Holmes, Phys. Technol., 16 (1985) 32.
4 C. S. Ha and W. J. Cho, Prog. Polym. Sci., 27 (2002) 759.
5 K. Van de Velde and P. Kiekens, Polymer Testing, 21 (2002) 433.
6 X. Shuai, F. E. Porbeni, M. Wei, T. Bullions and A. E. Tonelli, Macromolecules, 35 (2002) 3126.
7 A. A. Mansour, G. R. Saad and A. H. Hamed, Polymer, 40 (1999) 5377.
8 H. Marand, A. Alizadeh, R. Farmer, R. Desai and V. Velikov, Macromolecules, 33 (2000) 3392.
9 R. E. Withey and J. N. Hay, Polymer, 40 (1999) 5147.
10 Gazzano, M. L. Focarete, C. Reikel, A. Ripamonti and M. Scandola, Macromol. Chem. Phys., 202 (2001) 1405.
11 L. M. W. K. Gunaratne and R. A. Shanks, Thermochim. Acta, 430 (2005) 183.
12 P. S. Gill, S. R. Sauerbrunn and M. Reading, J. Thermal Anal., 40 (1993) 931.
13 J. E. K. Schawe, Thermochim. Acta, 260 (1995) 1.
14 B. Wunderlich, I. Okazaki, K. Ishikiriyama and A. Boller, Thermochim. Acta, 324 (1998) 77.
15 J. F. Turner, A. Riga, A. O'Connor, J. Zhang and J. Collis, J. Therm. Anal. Cal., 75 (2004) 257.
16 B. Wunderlich, A. Boller, I. Okazaki, K. Ishikiriyama, W. Chen, M. Pyda, J. Pak, I. Moon and R. Androsch, Thermochim. Acta, 330 (1999) 21.
17 S. L. Simon, Thermochim. Acta, 374 (2001) 55.
18 M. Sandor, N. A. Bailey and E. Mathiowitz, Polymer, 43 (2002) 279.
19 B. Wunderlich, J. Therm. Anal. Cal., 78 (2004) 7.
20 M. Reading and R. Luyt, J. Thermal Anal., 54 (1998) 535.
21 G. Amarasinghe, F. Chen, A. Genovese and R. A. Shanks, J. Appl. Polym. Sci., 90 (2003) 681.
22 K. Pielichowski, K. Flejtuch and J. Pielichowski, Polymer, 45 (2004) 1235.
23 L. M. W. K. Gunaratne, R. A. Shanks and G. Amarasinghe, Thermochim. Acta, 423 (2004) 127.
24 G. J. M. de Koning, P. J. Lemstra, D. J. T. Hill, T. G. Carswell and J. H. O'Donnell, Polymer, 33 (1992) 3295.
25 F. Biddlestone, A. Harris and J. N. Hay, Polym. Int., 39 (1996) 221.
26 P. J. Barham and A. Keller, J. Polym. Sci.: Polym. Phys. Edit., 24 (1986) 69.
27 L. L. Zhang, S. H. Goh, S. Y. Lee and G. R. Hee, Polymer, 41 (2000) 1429.
28 S. Gogolewski, M. Jovanovic, S. M. Perren, J. G. Dillon and M. K. Hughes, J. Biomed. Mater. Res., 27 (1993) 1135.
29 T. L. Bluhm, G. K. Hamer R. H. Marchessault, L. A. Fyfe and R. P. Veregin, Macromolecules, 19 (1986) 2871.
30 J. R. Knox, R. S. Portes and J. F. Johnson, Eds, Analytical Calorimetry, New York: Plenum Press, 1 (1968) 45.
31 Y. An, L. Dong, L. Li Z. Mo and Z. Feng, Eur. Polym. J., 35 (1999) 365.
32 M. Avrami, J. Chem. Phys., 8 (1939) 212.
33 M. Avrami, J. Chem. Phys., 9 (1941) 17.
34 S. Peng, Y. An, C. Chen, B. Fei, Y. Zhuang and L. Dong, Eur. Polym. J., 39 (2003) 1475.
35 P. J. Barham, J. Mater. Sci., 19 (1984) 3826.
36 W. D. Lee, E. S. Yoo and S. S. Im, Polymer, 44 (2003) 6617.
37 S. Z. D. Cheng and B. Wunderlich, Macromolecules, 21 (1988) 789.
38 D. Blundell and B. N. Osborn, Polymer, 27 (1986) 721.
39 Y. Lee and R. S. Porter, Macromolecules, 20 (1987) 1336.
40 R. Pearce and R. H. Marchessault, Polymer, 35 (1994) 3990.
41 V. B. F. Mathot (Ed.), Calorimetry and Thermal Analysis of Polymers, Hanser, New York 1993, Chapter 9, pp. 231–299.
42 S. Yamada, Y. Wang, N. Asakawa, N. Yoshie and Y. Inoue, Macromolecules, 34 (2001) 4659.
43 C. Chen, B. Fei, S. Peng, Y. Zhuang, L. Dong and Z. Feng, Eur. Polym. J., 38 (2002) 1663.
44 Y. Jin, J. Bonila, Y.G. Lin, J. Morgan, L. McCracken and J. Carnahan, J. Thermal Anal., 46 (1996) 1047.
45 B. B. Sauer, W. G. Kamper, E. N. Blanchard, S. A. Threefoot and B. S. Hsiao, Polymer, 41 (2000) 1099.
46 W. G. Kampert and B. B. Sauer, Polymer, 42 (2001) 8703.

Received: January 20, 2005
Accepted: June 23, 2005

DOI: 10.1007/s10973-005-6872-8